Understanding the Role of Solvent on Regulating Crystal Habit

Xiongtao Ji[a], Jingkang Wang [a,b,c], Ting Wang [a,b,c*], Xin Huang [a,b,c], Xin Li[a], Na Wang[a], Yunhai Huang[a], Rui Li[a], Bugui Zhao[d], Tao Zhang[d], Hongxun Hao[a,b,c*]

[a] National Engineering Research Center of Industrial Crystallization Technology, School of Chemical Engineering and Technology, Tianjin University, Tianjin 300072, China

[b] Collaborative Innovation Center of Chemical Science and Engineering (Tianjin), Tianjin 300072, China

[c] State Key Laboratory of Chemical Engineering, School of Chemical Engineering and Technology, Tianjin University, Tianjin 300072, China

[d] Shandong Lukang Pharmaceutical Co., Ltd, Shandong 272021, China

Table S1 Crystallographic information for the cefradine

Crystal data	
Chemical formula	$C_{16}H_{19.67}N_3O_{4.33}S$
M_r	355.41
Crystal system, space group	Monoclinic, *I*2
Temperature (K)	293
a, *b*, *c* (Å)	16.8521 (4), 11.9552 (2), 26.6656 (6)
β (°)	108.107 (3)
V (Å^3)	5106.3 (2)
Z	12
Radiation type	Cu *K*α
μ (mm^{-1})	1.94
Crystal size (mm)	0.25 × 0.23 × 0.20
Data collection	
Diffractometer	Bruker Smart Apex CCD area detector
Absorption correction	Multi-scan SADABS
T_{min}, T_{max}	0.632, 0.935
No. of measured, independent and observed [$I > 2\sigma(I)$] reflections	17284, 8354, 7909
R_{int}	0.027

$(\sin \theta/\lambda)_{max}$ (Å^{-1})	0.597
Refinement	
$R[F^2 > 2\sigma(F^2)]$, $wR(F^2)$, S	0.053, 0.152, 1.03
No. of reflections	8354
No. of parameters	670
No. of restraints	191
H-atom treatment	H atoms treated by a mixture of independent and constrained refinement
$\Delta\rho_{max}$, $\Delta\rho_{min}$ (e Å^{-3})	0.75, −0.51
Absolute structure	Flack x determined using 3082 quotients [(I+)-(I-)]/[(I+)+(I-)] (Parsons, Flack and Wagner, Acta Cryst. B69 (2013) 249-259).
Absolute structure parameter	0.008 (11)

Computer programs: SHELXT 2018/2 (Sheldrick, 2018), SHELXL2018/3 (Sheldrick, 2018).

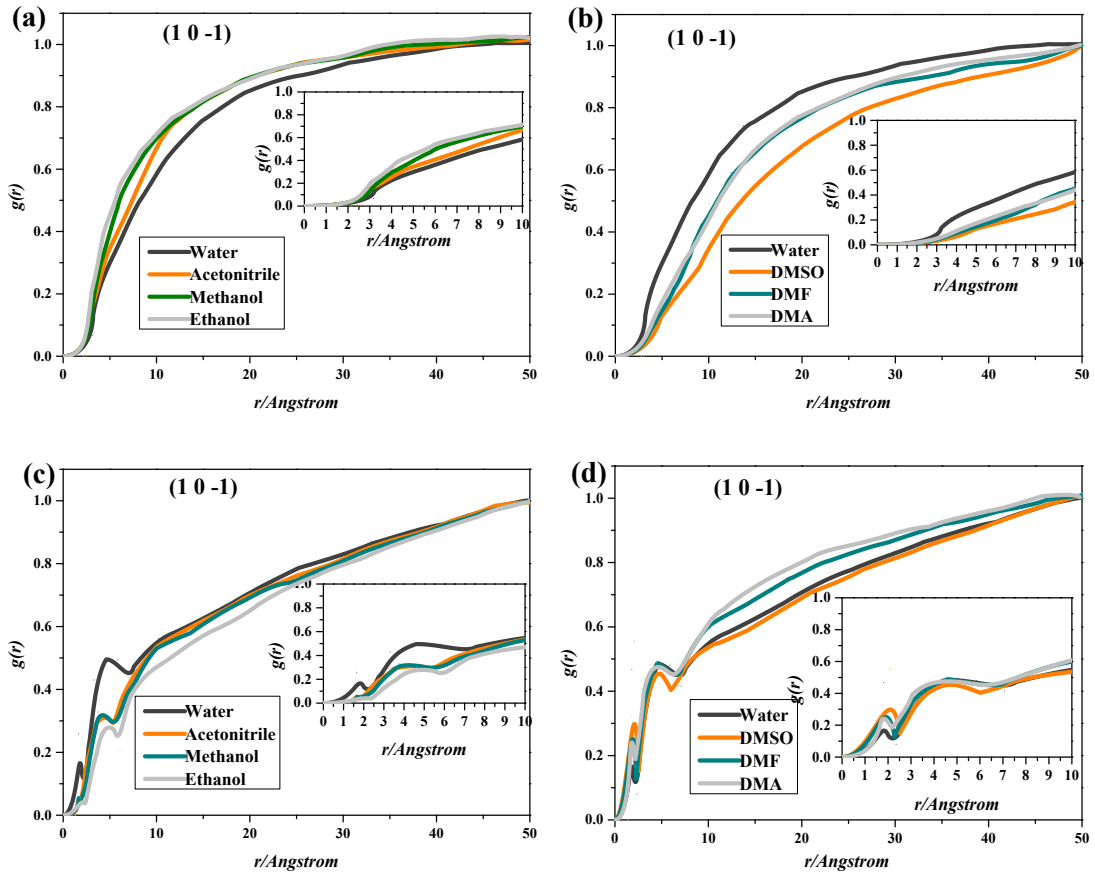

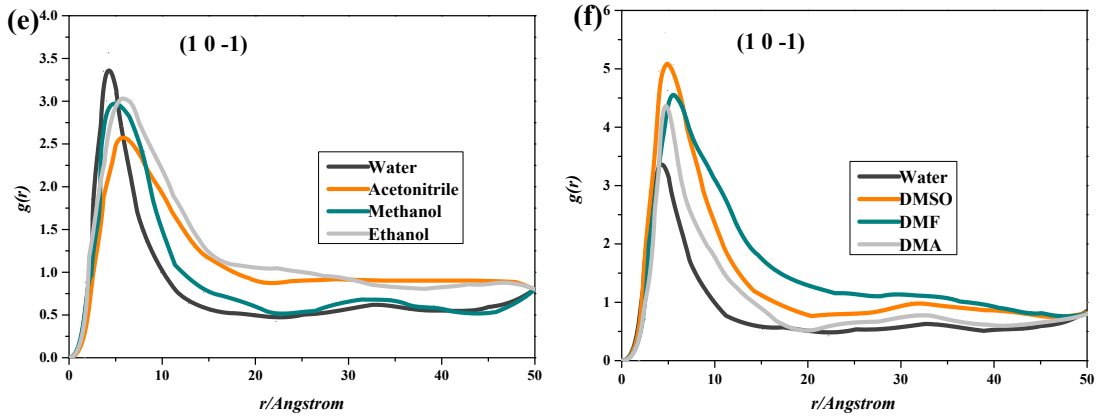

Fig.S1. Radial distribution functions *g(r)* around the interfacial layers of (10-1). (a) Represents radial distribution functions *g(r)* of solute (group 1) around the interfacial layers; (b) represents radial distribution functions *g(r)* of solute (group 2) around the interfacial layers; (c) represents radial distribution functions *g(r)* of solvent (group 1) around the interfacial layers; (d) represents radial distribution functions *g(r)* of solvent (group 2) around the interfacial layers; (e) represents radial distribution functions *g(r)* of solute around solvent (group 1); (f) represents radial distribution functions *g(r)* of solute around solvent (group 2).

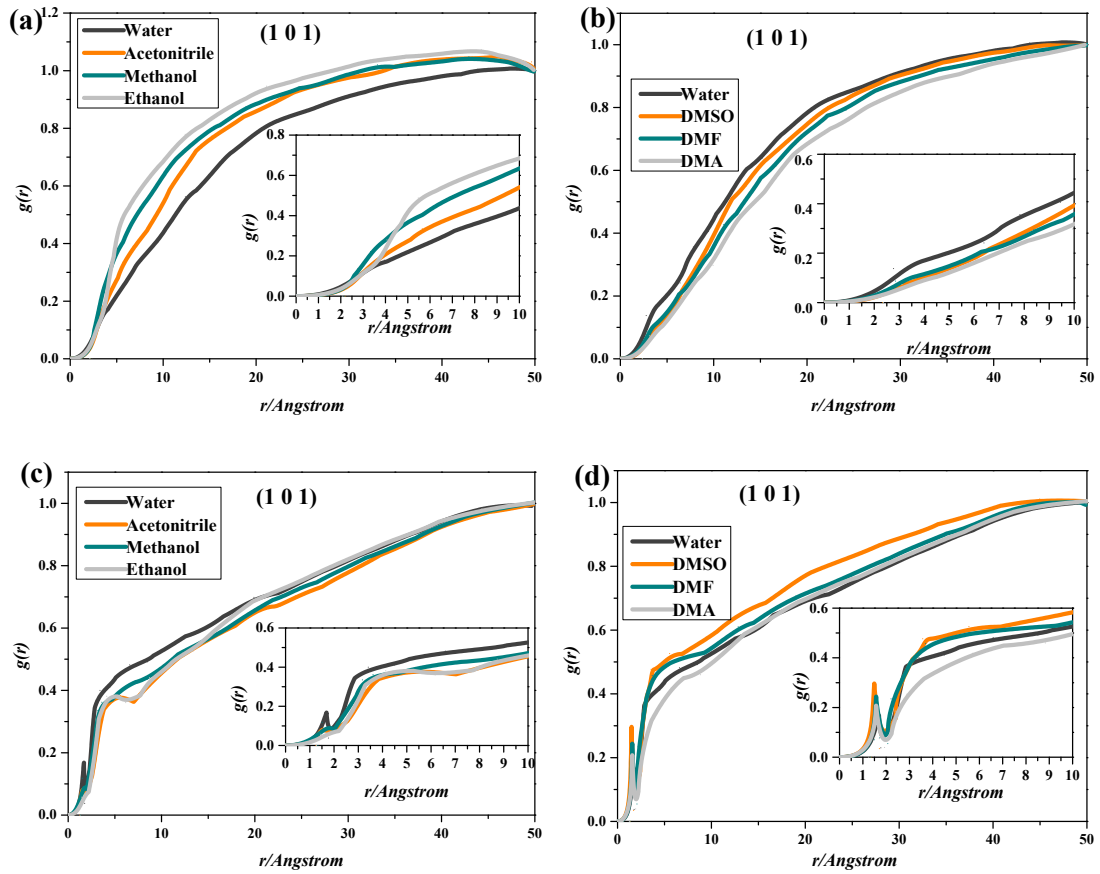

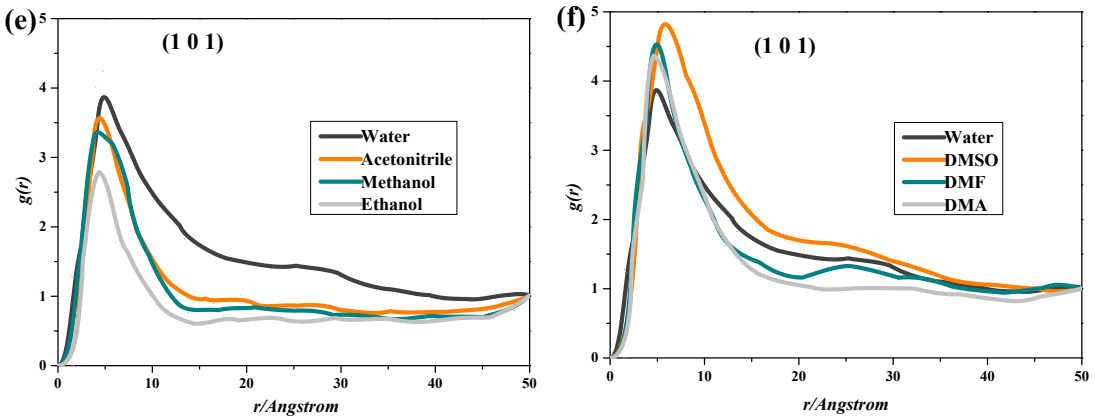

Fig.S2. Radial distribution functions *g(r)* around the interfacial layers of (101). (a) Represents radial distribution functions *g(r)* of solute (group 1) around the interfacial layers; (b) represents radial distribution functions *g(r)* of solute (group 2) around the interfacial layers; (c) represents radial distribution functions *g(r)* of solvent (group 1) around the interfacial layers; (d) represents radial distribution functions *g(r)* of solvent (group 2) around the interfacial layers; (e) represents radial distribution functions *g(r)* of solute around solvent (group 1); (f) represents radial distribution functions *g(r)* of solute around solvent (group 2).

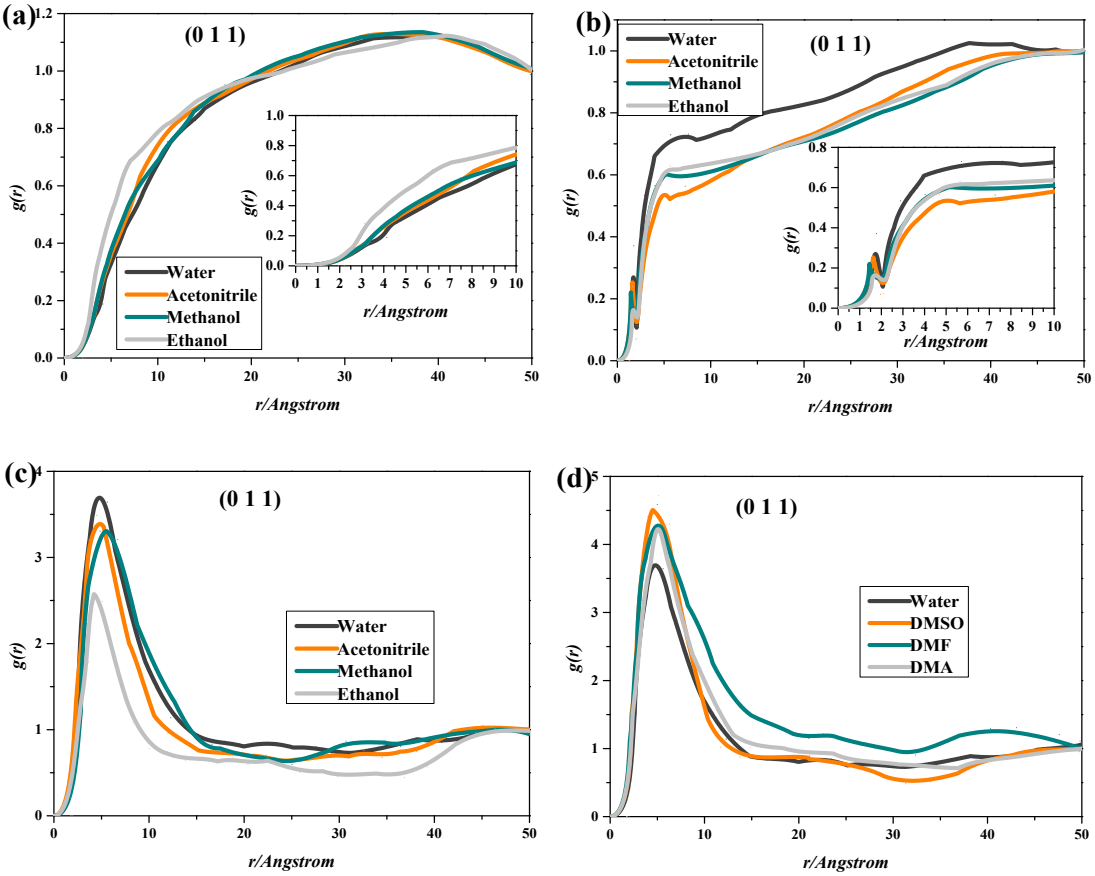

Fig.S3. Radial distribution functions *g(r)* around the interfacial layers of (011). (a) Represents radial distribution functions *g(r)* of solute (group 1) around the interfacial layers; (b) represents radial distribution functions *g(r)* of solvent (group 1) around the interfacial layers; (c) represents

radial distribution functions *g(r)* of solute around solvent (group 1); (d) represents radial distribution functions *g(r)* of solute around solvent (group 2).

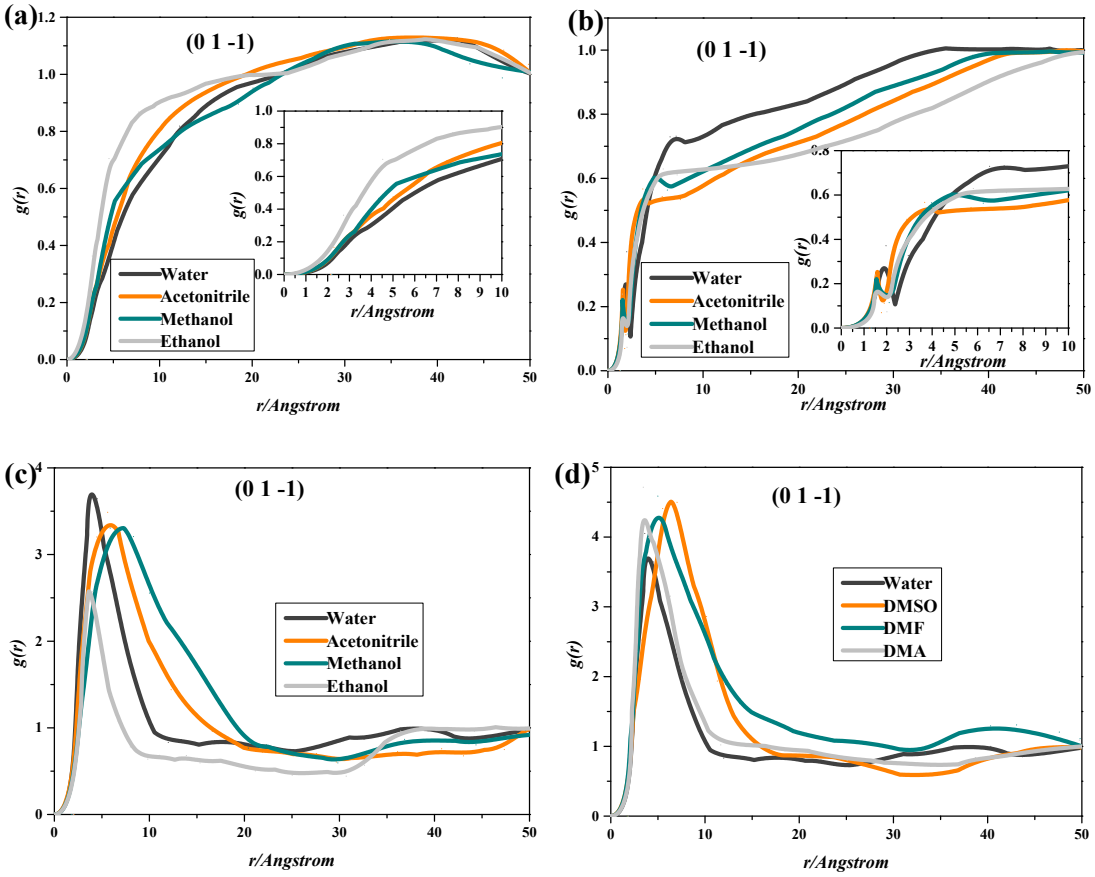

Fig.S4. Radial distribution functions *g(r)* around the interfacial layers of (01-1). (a) Represents radial distribution functions *g(r)* of solute (group 1) around the interfacial layers; (b) represents radial distribution functions *g(r)* of solvent (group 1) around the interfacial layers; (c) represents radial distribution functions *g(r)* of solute around solvent (group 1); (d) represents radial distribution functions *g(r)* of solute around solvent (group 2).

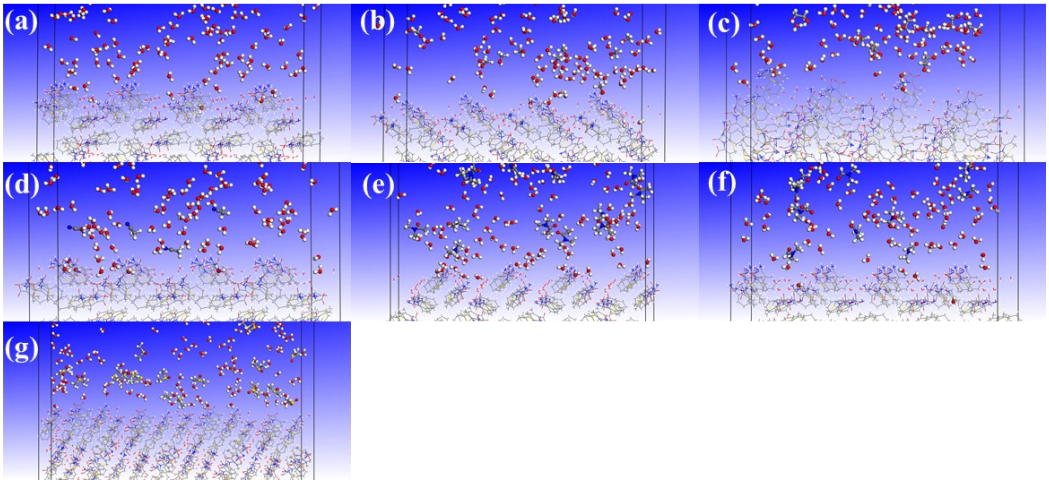

Fig.S5. Snapshot of water (a), methanol (b), ethanol (c), acetonitrile (d), DMA (e), DMF (f) and DMSO (g) on the (10-1) face at 293.15 K at 500 ps (solute molecules were removed for clarity).

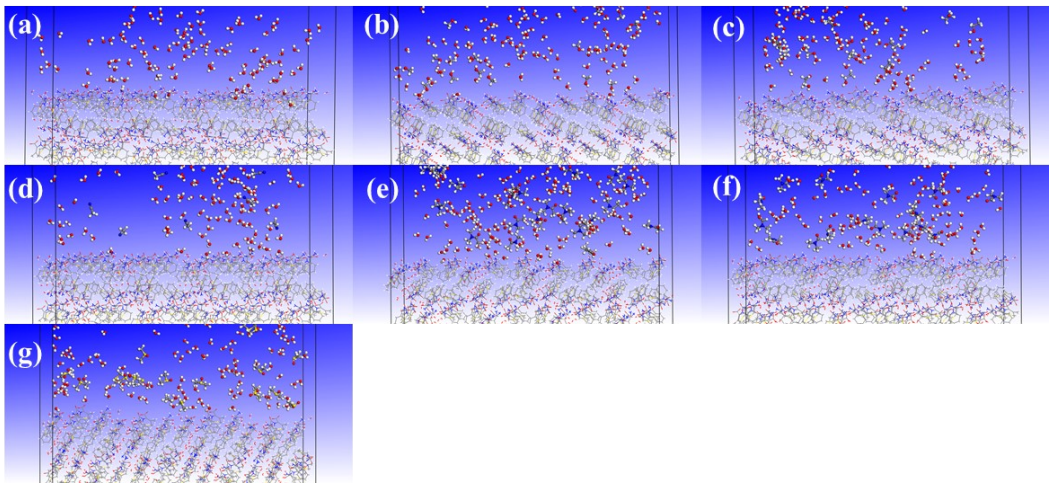

Fig.S6. Snapshot of water (a), methanol (b), ethanol (c), acetonitrile (d), DMA (e), DMF (f) and DMSO (g) on the (101) face at 293.15 K at 500 ps (solute molecules were removed for clarity).

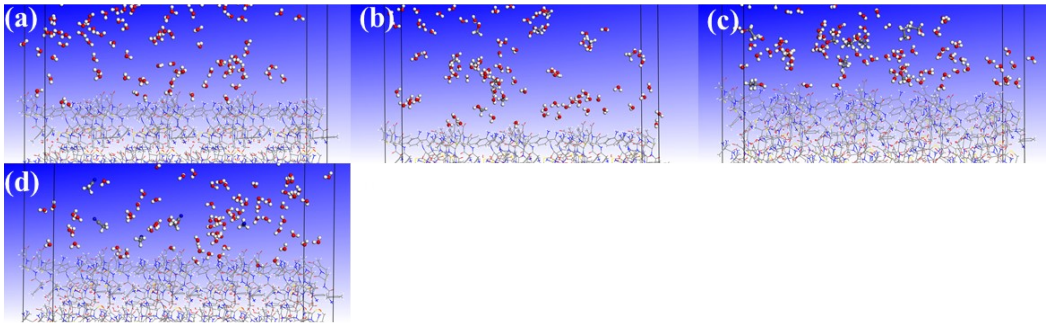

Fig.S7. Snapshot of water (a), methanol (b), ethanol (c) and acetonitrile (d) on the (10-1) face at 293.15 K at 500 ps (solute molecules were removed for clarity).

Table S2 Peak finding reports of cefradine dehydrate (Deposition Number 963812 in CCDC)

#	2-Theta	d(A)	BG	Height	I%	Area	I%	FWHM
1	7.603	11.6183	15	7574	76.2	55076	78.6	0.124
2	14.302	6.1877	17	6342	63.8	46739	66.7	0.125
3	14.76	5.9967	48	2122	21.4	16320	23.3	0.131
4	17.419	5.0868	14	4728	47.6	33761	48.2	0.121
5	19.962	4.4442	45	2956	29.8	20350	29.1	0.117
6	23.402	3.7981	61	2268	22.8	17520	25	0.131
7	23.702	3.7508	157	2202	22.2	14139	20.2	0.109
8	24.337	3.6543	184	4441	44.7	27607	39.4	0.106
9	25.017	3.5565	255	4202	42.3	26205	37.4	0.106
10	25.582	3.4792	173	1468	14.8	35325	50.4	0.409
11	25.798	3.4506	95	6449	64.9	47348	67.6	0.125
12	26.039	3.4192	49	3891	39.2	48846	69.7	0.213

13	27.879	3.1976	38	1601	16.1	15690	22.4	0.167
14	28.878	3.0892	78	2509	25.3	17801	25.4	0.121

Table S3 Peak finding reports of theoretical monoclinic form (Deposition Number 2116441 in CCDC)

#	2-Theta	d(A)	BG	Height	I%	Area	I%	FWHM
1	5.479	16.1175	36	2759	31.4	20958	29.1	0.129
2	7.242	12.1963	36	8793	100	71922	100	0.139
3	10.881	8.1244	8	1865	21.2	16474	22.9	0.15
4	16.359	5.4142	54	6591	75	57082	79.4	0.147
5	20.219	4.3884	90	1835	20.9	16219	22.6	0.15
6	20.839	4.2591	100	1152	13.1	19547	27.2	0.288
7	23.039	3.8572	59	1990	22.6	15781	21.9	0.135
8	24.679	3.6044	59	1641	18.7	26736	37.2	0.277
9	27.46	3.2454	44	641	7.3	20392	28.4	0.541
10	27.799	3.2066	44	443	5	14625	20.3	0.561
11	28.442	3.1356	99	1323	15	15145	21.1	0.195

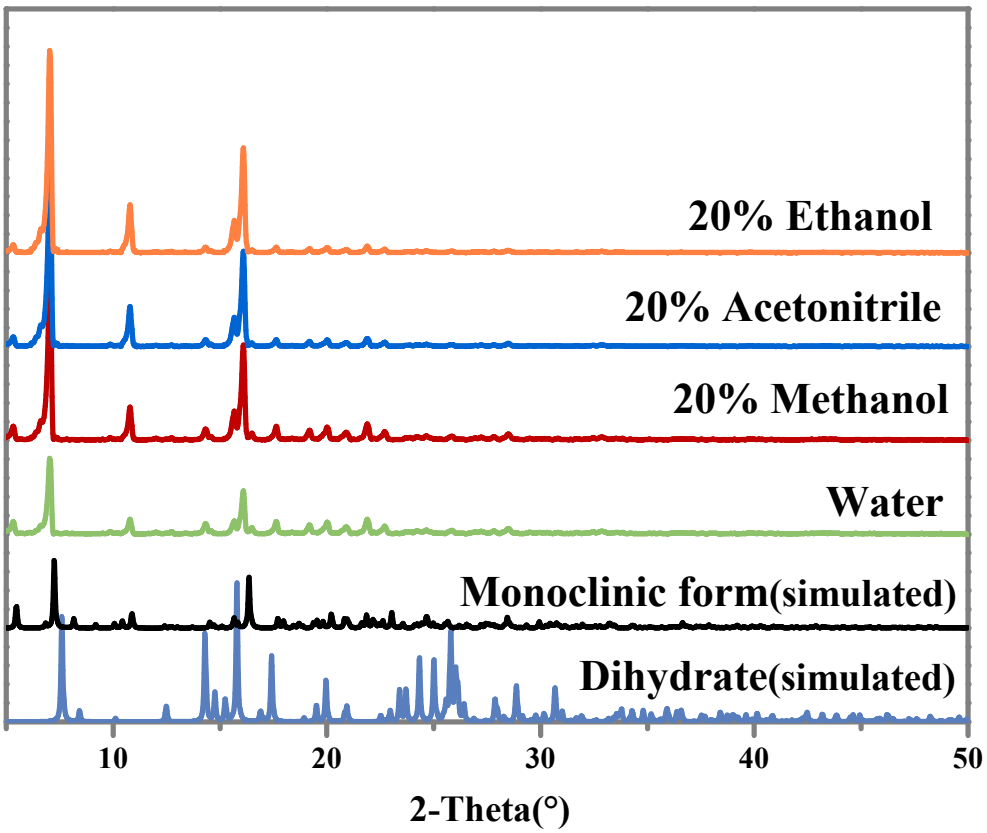

Fig.S8. PXRD patterns of theoretical crystals and crystals obtained from group 1.

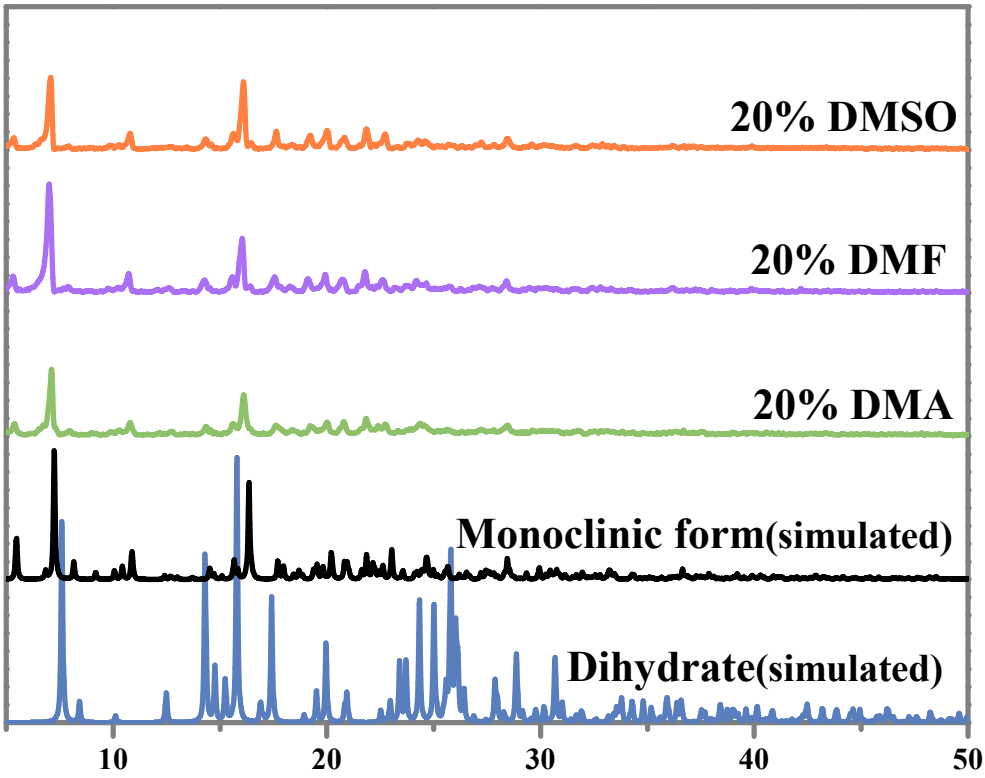

Fig.S9. PXRD patterns of theoretical crystals and crystals obtained from group 2.

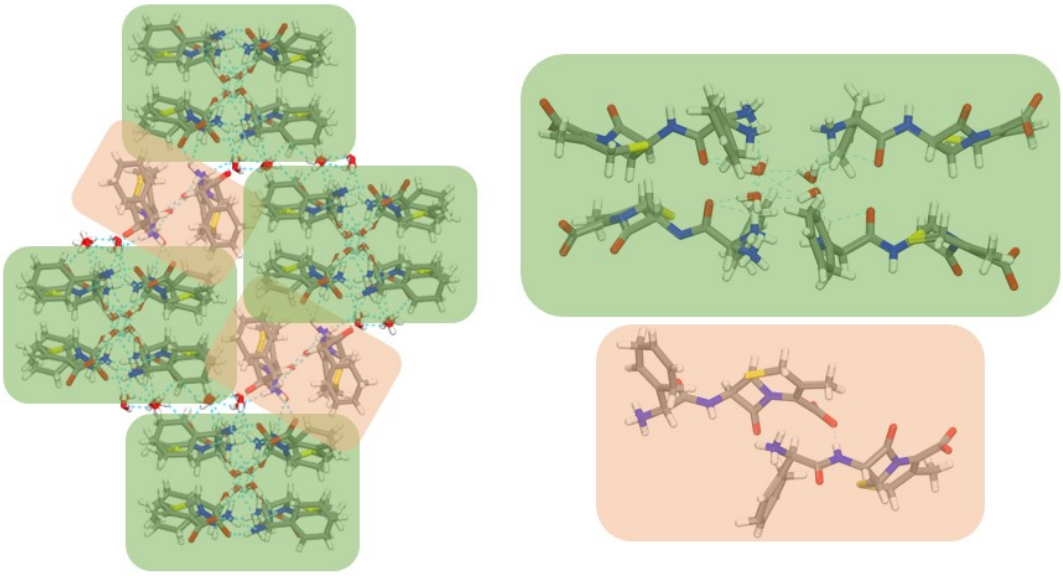

Fig.S10. The crystal structure of monoclinic form.

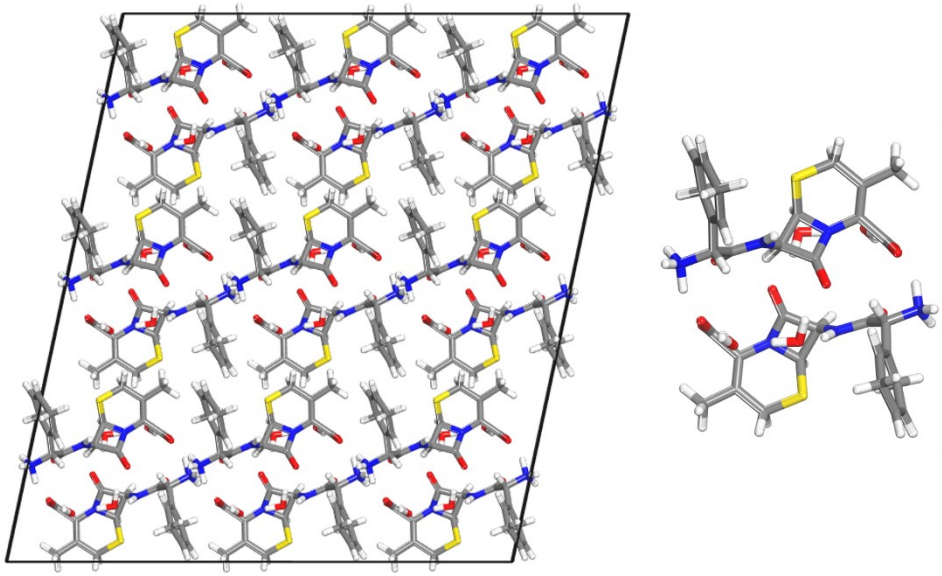

Fig.S11. The crystal structure of cefradine dihydrate.

Table S4 Adsorption energies (kcal/mol^{-1}) of individual solvent molecules onto morphologically important crystal faces of cefradine based on the previous structure (CCDC no. 2019845).

		(1 0 -1)	(1 0 1)	(0 1 1)	(0 1 -1)
Control	Water	-10.4	-11.8	-12.9	-12.8
Group 1	Methanol	-9.15	-10.5	-11.4	-11.6
	Ethanol	-8.29	-9.92	-11.2	-11.3
	Acetonitrile	-10.0	-11.3	-12.1	-12.8
Group 2	DMF	-10.6	-14.6	-17.4	-18.4
	DMA	-11.3	-14.6	-16.9	-17.9
	DMSO	-12.8	-15.2	-18.3	-18.5

S1. Distribution of cefradine while triethylamine was added

According to previous work, Fig.S12 plots the distribution of the three forms of cefradine as a function of pH in water. The activity of A increases first and then decreases with the increasing of pH and there is a maximum value at the isoelectric point (pH=5.0). With the addition of triethylamine, the pH of the solution gradually increased from acidic to isoelectric point, and the cation of cefradine gradually becomes the neutral molecular. The supersaturation adjusted by triethylamine was used as the driving force for crystal growth, and the neutral molecules produced were used as raw materials for crystal growth.

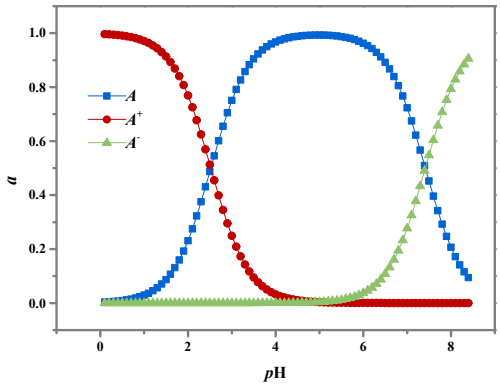

Fig.S12 Distribution curve of three existing forms of cefradine in methanol with *p*H. and A^+, A and A^- represent the cation, zwitterion and anion of cefradine

S2. Details of MD simulation

Before simulations, all the crystal surfaces with vacuum slab and boxes of solution were optimized to make sure the structures were completely relaxed. During simulations, the crystal structure was kept fixed. The Condensed-phase Optimized Molecular Potentials for Atomistic Simulation Studies (COMPASS) force field (with force field-assigned partial atomic charges) was used to model atomic interactions in the crystal structure of cefradine, solvents and others. All the systems were initially subjected to energy minimization in order to avoid unwanted overlap between the atoms and to reduce the thermal noise in the system; then velocities were generated according to the Maxwell–Boltzmann distribution. Finally, isothermal and isochoric (NVT) MD simulations were conducted at 293.15 K. The temperature was controlled by the Nose–Hoover thermostat with a relaxation time of 0.1 ns, and Ewald summation was used to incorporate the long-range interactions. The equations of motion were integrated by the Verlet velocity algorithm with a time step of 1 fs for a simulation duration of 500 ps, and trajectories were saved at every 0.5 ps. The equilibration state was determined by observing the change in the thermodynamic

properties such as energy and temperature as a function of time. It was found that all the systems reach equilibrium within 100 ps of simulation; thus all the properties were estimated using trajectory after 100 ps. All the MD simulations were performed in Materials Studio (Version 7.0).